Fabrication and mechanical properties of Ti_2AlN/TiAl composite with continuous network structure

JIANG, Min jin; SUN, Hong liang; LIU, Rui; JIANG, Xiao song; ZHANG, Ya li; SUN, Da ming

Published in:
Transactions of Nonferrous Metals Society of China (English Edition)

DOI (link to publication from Publisher):
10.1016/S1003-6326(23)66194-1

Publication date:
2023

Document Version
Publisher's PDF, also known as Version of record

Available online at www.sciencedirect.com
ScienceDirect
Trans. Nonferrous Met. Soc. China 33(2023) 1437−1451
Transactions of Nonferrous Metals Society of China
www.tnmsc.cn

Fabrication and mechanical properties of Ti_2AlN/TiAl composite with continuous network structure

Min-jin JIANG[1,2], Hong-liang SUN[1,2], Rui LIU[1,2], Xiao-song JIANG[1,2], Ya-li ZHANG[3], Da-ming SUN[4]

1. Key Laboratory of Advanced Technologies of Materials, Ministry of Education, Chengdu 610031, China;
2. School of Materials Science and Engineering, Southwest Jiaotong University, Chengdu 610031, China;
3. School of Mechanical Engineering, Sungkyunkwan University,
2066 Seobu-ro, Jangan-gu, Suwon-si, Gyeonggi-do, 16419, Korea;
4. Department of Chemistry and Bioscience, Aalborg University, Aalborg, 9220, Denmark

Received 14 December 2021; accepted 6 June 2022

Abstract: Nitrogen was introduced into TiAl pre-alloyed powder using high-temperature gas nitriding, and Ti_2AlN/TiAl composites with a continuous network structure of the reinforced phase were prepared via spark plasma sintering. The results show that the hardness of the composite is significantly higher than that of TiAl alloy, and increases with the increase of nitriding time. The strengthening effect is originated from the synergistic effect of the solid-solution strengthening caused by the nitriding of the powder, the continuous network of the Ti_2AlN phase with high hardness and elastic modulus, and the increase of dislocation density. Additionally, the compressive strength of the Ti_2AlN/TiAl composites is lower than that of the TiAl alloy, which is related to a part of Ti_2AlN particles that are directly formed after nitriding and excessive reinforcement content.

Key words: pre-alloyed powder; nitriding; Ti_2AlN/TiAl composite; continuous network structure; microstructure; mechanical properties

1 Introduction

Owing to the ordered structure and covalent bonding of Ti–Al intermetallic compounds [1], TiAl alloys possess the advantages of low density, high specific strength, excellent high-temperature creep performance, and high-temperature oxidation resistance. The above advantages enabled wide application prospect of TiAl alloys in aero-engine and automotive fields, particularly in aircraft turbine blades, turbine disks, high-pressure compression turbines, automobile exhaust valves, and other components [2]. However, the lack of room-temperature plasticity, fracture toughness and elevated temperature strength of TiAl alloys limits their further development and application [3]. At present, considerable research efforts have been focused on improving the comprehensive mechanical properties of TiAl alloys using heat treatment, alloying, composite strengthening, ultrafine grains, and regulating phase composition and distribution; these studies yielded many important results [4−8]. Among the above methods, the composite strengthening method can be used to obtain excellent comprehensive mechanical properties and therefore, widely used to optimize the properties of TiAl alloys. For example, YANG et al [9] successfully prepared Ti_2AlC-reinforced TiAl composites via spark plasma sintering using Ti powder, Al powder, and carbon nanotubes as raw materials, improving the compressive yield strength

Corresponding author: Hong-liang SUN, Tel/Fax: +86-28-87634177, E-mail: sunhl@swjtu.edu.cn;
Xiao-song JIANG, Tel/Fax: +86-28-87634177, E-mail: xsjiang@swjtu.edu.cn
DOI: 10.1016/S1003-6326(23)66194-1

and hardness of the sintered samples to 2058 MPa and 6.12 GPa, respectively. TAN et al [10] produced a Ti_2AlN/TiB/TiAl composite via the addition of BN particles and arc melting, significantly improving the compressive strength of the TiAl alloy without reducing the compressive strain.

In terms of the selection of the reinforced phase, ternary layered compounds, with properties of both metals and ceramics, are widely used as the reinforced phase in various composites [11]. The general formula of ternary layered compounds is $M_{n+1}AX_n$ (where M represents an early transition metal, A represents IIIA or IVA group elements, and X represents nitrogen or carbon) [12]. Common representatives include Ti_2AlC and Ti_2AlN, among which Ti_2AlN has a higher hardness and elastic modulus [13], and its thermal expansion coefficient is closer to that of TiAl [14]. Thus, Ti_2AlN is more suitable as a reinforced phase for TiAl-based composites. In situ synthesis of the reinforced phase can eliminate some material interface problems, such as brittle layer and wettability [15]. Inspired by honeycomb structures [16] and hard biomaterials [17], a large number of researchers have studied new composites with uniform continuous network structures of the reinforced phase. For example, HUANG et al [18] obtained excellent mechanical properties and oxidation resistance through the design of TiC/Ti6Al4V network-structured composites. JIAO et al [19] changed the reinforced phase structure from isolated particles to a continuous network by increasing the volume fraction of TiB_w, resulting in excellent tensile and creep properties of the composites. Moreover, compared with other in situ sintering methods, spark plasma sintering (SPS) is an efficient and reliable technology for sintering refractory intermetallic compounds [20]. For example, VOISIN et al [21] successfully prepared a TiAl turbine blade with the near-net shape using SPS of TiAl pre-alloyed powder.

At present, the research on the in situ synthesis of TiAl matrix composites by powder metallurgy mainly focuses on the preparation of TiAl matrix composites by mixed element powder sintering [22−25]. However, less attention to the research on the preparation of TiAl matrix composites using TiAl pre-alloyed powder has been paid. Therefore, in this study, Ti_2AlN/TiAl composites with a new continuous network structure were successfully prepared via in situ reaction with TiAl pre-alloyed powder as raw material, high temperature gas nitriding and SPS sintering. The microstructure, high temperature hardness and room temperature compression properties of Ti_2AlN/TiAl composites were analyzed. In addition, the relationship between the uniform continuous network reinforced phase structure on the high-temperature hardness and room-temperature compression properties of the Ti_2AlN/TiAl composites was determined.

2 Experimental

The raw material was a TiAl pre-alloyed powder (Ti−48Al−2Cr−2Nb, approximately 150 μm). Figure 1 shows a schematic of material preparation divided into three steps. The first step was ball milling and refining of the TiAl pre-alloyed powder using a planetary ball mill. The TiAl pre-alloyed powder was ball-milled and mixed for 6 h at a speed of 350 r/min. Figures 1(a, b) show the ball milling and nitriding processes of the pre-alloyed powder, respectively. The second step was to nitride

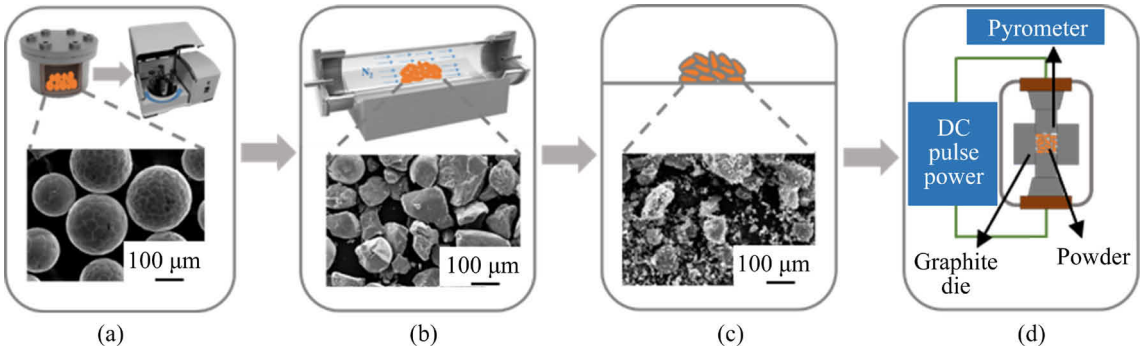

Fig. 1 Preparation process of Ti_2AlN/TiAl composite: (a) Ball milling of TiAl pre-alloy powder; (b) Nitriding of TiAl pre-alloy powder; (c) Nitrided TiAl pre-alloy powder; (d) Spark plasma sintering

the refined powder in a tubular furnace at 900 °C with a nitrogen flow rate of 25 mL/min. The morphology of the powder after nitriding is shown in Fig. 1(c). In the third step, SPS was used for sintering and forming, and the operating principles of the SPS equipment are shown in Fig. 1(d). The nitrided powder was placed in a graphite mold and sintered under vacuum at 1250 °C and 40 MPa for 5 min. In this study, the nitrogen content of the TiAl pre-alloyed powder was controlled by the nitriding time. To explore the effect of nitriding time on the microstructure and mechanical properties of Ti_2AlN/TiAl composites, the nitriding time gradient was set to be 0, 2, 4, and 8 h; thus, the corresponding Ti_2AlN/TiAl composites sintered at different nitriding time were denoted as TAN-0 h, TAN-2 h, TAN-4 h, and TAN-8 h, respectively.

The hardness values at different temperatures were measured using a high-temperature hardness tester (HVT−1000) under low vacuum condition, 50 N load, and 15 s holding time. The selected test temperature gradients were 25, 200, 400, 600, 700, and 800 °C, and a low vacuum was used to prevent damage to the indenter and sample caused by high-temperature oxidation. The hardness data under each variable must be measured at least 5 times, and the indentation should be checked by metallographic microscope after the measurement. If the indentation is limited to the interior of a single particle, the hardness data should be tested and measured again to ensure the accuracy of the hardness data.

The phase compositions of the Ti_2AlN/TiAl composites and pre-alloyed powder were determined using Cu K_α X-ray diffraction (XRD) with the scanning range of 10°−90° and step size of 0.02°. The nitrogen content of the powder was determined using an oxygen−nitrogen−hydrogen analyzer (ONH836), and the mass of each test powder was approximately 0.1 g. The microstructures of the composites were observed using scanning electron microscopy (SEM, SUPAR 55 SAPPHIRE) in the backscattered electron mode. The phase composition was further analyzed using energy dispersive spectroscopy (EDS). The microstructures of the composites were characterized using transmission electron microscopy (TEM, TALOS F200X). The microscopic characteristics of the enhanced phase were further studied using selected area electron diffraction (SAED) and high-resolution TEM (HRTEM). The fracture morphology was observed using SEM to analyze the fracture mechanism. The cross-section of the fracture sample was etched in an HF−HNO_3−H_2O solution (5:5:90 in vol.%) to better observe the section morphology near the fracture and explore the characteristics of crack initiation and propagation.

3 Results

3.1 Microscopic characteristics

Figure 2 shows the micromorphology and energy spectrum of the powder before and after nitriding. As shown in Fig. 2(a), ball milling resulted in the breaking of particles into fine-grained structures with different shapes, causing the accumulation of powder particle defects, thus enhancing the diffusion of the powder and was conducive to subsequent nitriding [26,27]. At the same time, the size of the TiAl pre-alloyed powder decreased, conducive to the densification of TAN composites and the improvement of the properties of TAN composites [28]. Figure 2(b) shows the powder morphology after nitriding: white flocks were evenly distributed on the powder surface. The

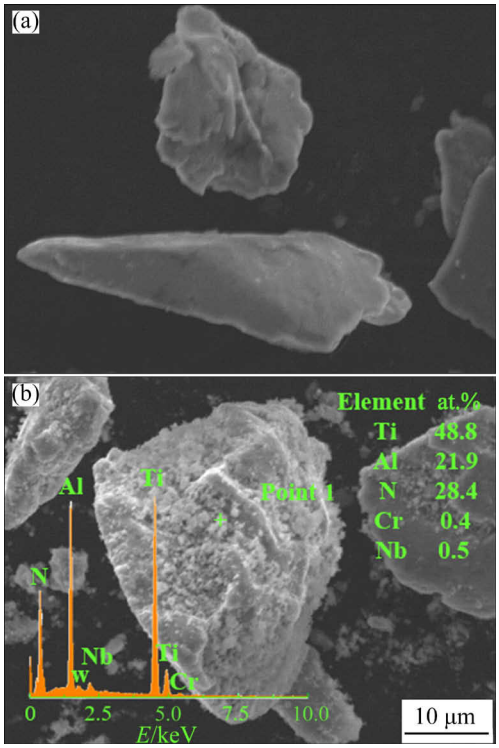

Fig. 2 Micromorphology and energy spectrum of TiAl pre-alloy powder after ball milling: (a) Before nitriding; (b) After nitriding

results at Point 1 showed that N appeared in this characteristic area, implying the successful formation of nitride layer on the surface of the TiAl pre-alloyed powder particles by high-temperature nitriding in N_2 atmosphere.

The XRD results for the TiAl pre-alloyed powder before and after nitriding are shown in Fig. 3. Figure 3(a) shows the XRD patterns of the TiAl pre-alloyed powder at different nitriding time, indicating that the phase composition of the powder before nitriding was TiAl, and a new characteristic peak appeared after nitriding. The XRD results and literature [29] suggested that the new characteristic peak corresponded to the TiN and Ti_2AlN phases formed after powder nitriding. Figure 3(b) shows an enlarged image of the strongest characteristic peak region of the TiAl phase in Fig. 3(a), showing that after nitriding, the position of the strongest characteristic peak slightly shifted to a lower diffraction angle, similar to the results obtained by BARS et al [30]. This result implied that nitrogen atoms diffused into the TiAl lattice and a solid solution conducive to improving the material properties was formed.

WANG et al [31] found that the solid solution of nitrogen atoms in Ti powder was formed after high-temperature nitriding for 0.5 h, while the minimum nitriding time was 2 h. Therefore, a sufficient amount of solid solution was formed during the nitriding of the TiAl pre-alloyed powder for 2 h. This conclusion is consistent with the result that there is little difference in the shift of the main peak position caused by the solid solution in Nitriding-2 h, Nitriding-4 h, and Nitriding-8 h samples in Fig. 3(b). According to a study by ROY et al [32], when nitrogen concentration was higher than the solid solubility of N in TiAl, the nitride phase began to form on the powder surface, as seen in Fig. 3(a). The TiN phase was formed in the powder after nitriding for 2 h, but the characteristic peak intensities of TiN and Ti_2AlN were small after nitriding for 2 and 4 h, attributed to the short nitriding time and insufficient diffusion between the active nitrogen and alloy powder at high temperatures. With an increase in nitriding time, the intensities of the characteristic peaks of TiN and Ti_2AlN increased. Especially after nitriding for 8 h, the intensity of the characteristic peaks of the TiN and Ti_2AlN phases was several times higher than that before nitriding, indicating that the alloy powder diffused sufficiently at this nitriding time. Therefore, it can be concluded that the nitriding of the TiAl pre-alloyed powder can be divided into two processes: a small number of N atoms enter the lattice of γ-TiAl to produce a solid solution, and then the excessive N forms TiN and Ti_2AlN on the powder surface. At the same time, the nitriding time determines the yield of reaction products.

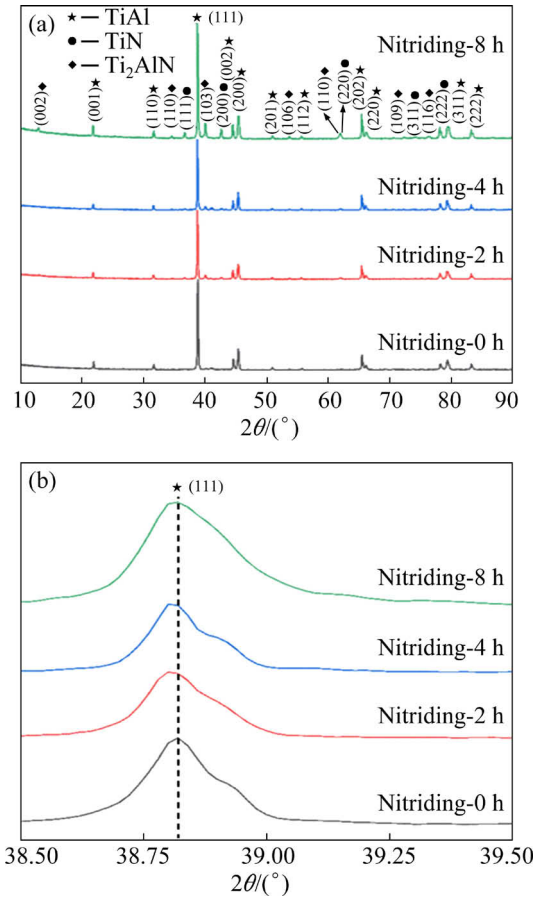

Fig. 3 XRD patterns of different samples: (a) TiAl pre-alloy powder at different nitriding time; (b) Enlarged region of strongest diffraction peak of TiAl pre-alloyed powder

It is worth noting that the TiAl phase is still the main phase in all titanium aluminum nitride pre-alloyed powders, indicating the retention of a large number of the original TiAl phases throughout nitriding. The TiN phase formed on the powder surface is the key raw material for the in situ generation of the continuous network of the reinforced phase, whereas Ti_2AlN produced during nitriding may act as the reinforced phase. Prior research [25,33] showed that the continuous network of Ti_2AlN produced by in situ reaction during sintering has a greater strengthening effect

than the directly added reinforced phase: the latter improves the hardness and strength but also reduces the plasticity of the material. Excessive reinforced phase may also increase material brittleness and reduce its strength. Therefore, studies on nitriding should avoid the direct formation of Ti_2AlN particles as much as possible, and more N atoms should be introduced in the form of a solid solution or TiN. The nitrided TiAl pre-alloyed powder is hereafter referred to as TiAl(N) powder.

XRD patterns of the TAN composites are shown in Fig. 4. Several characteristic peaks appeared in the composite TAN-0 h, corresponding to the Ti_3Al phase by qualitative analysis. These characteristic peaks were formed because the sintering temperature exceeded 1125 °C (eutectoid reaction temperature of the TiAl alloy) [34], and the Ti_3Al phase was formed during furnace cooling. At the same time, the TiN phase obtained by powder nitriding disappeared after sintering, indicating that the TiN phase underwent an in situ reaction during SPS sintering and was completely consumed to form a Ti_2AlN strengthened phase [35]. Similarly, the Ti_3Al phase transformed during cooling.

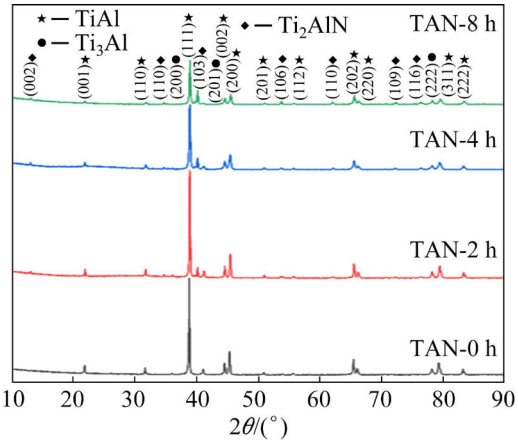

Fig. 4 XRD patterns of TAN composites at different nitriding time

As seen from the characteristic peak of the phase composition in Fig. 4, with the increase in nitriding time, the content of the Ti_2AlN strengthened phase increases, while the contents of TiAl and Ti_3Al phases continue to decrease, especially the content of the Ti_3Al phase in TAN-8 h. This result shows that with the increase in nitriding time, the content of the TiN phase in the powder increases. Therefore, in the in situ reaction, a greater amount of the TiAl phase reacts with the TiN phase to form the Ti_2AlN-reinforced phase [36], leading to the reduction in the amount of the TiAl phase and the Ti_3Al phase precipitated during cooling.

The microstructures of the TAN composites are shown in Fig. 5. No obvious pores were observed on the composite surface, consistent with the high density of the composite. As shown in Figs. 5(a, b), the TAN-0 h composite was mainly composed of equiaxed γ grains and γ/α lamellae, into which equiaxed α and γ transformed at high temperatures during cooling. At the same time, owing to the mutual pinning of α and γ and rapid SPS sintering, the grain growth was slow and insufficient; therefore, the grain size obtained in Fig. 5 is small, 10−40 μm [37]. Similarly, because TiAl was still the main phase of the nitrided powder, the microstructures of the other three composites also contained the same two-state structure, as shown in Figs. 5(d−f), respectively.

The microstructure of the TAN-2 h composite was assessed using energy spectrum analysis to determine the composition of different contrast phases. The analysis results are shown in Figs. 5(g−i). Figure 5(g) shows the molar fraction of the dark gray phase (Point 1) in Fig. 5(c), in which the molar ratio of Ti:Al:N is approximately 2:1:1. Combined with the XRD analysis results, this phase is a Ti_2AlN-strengthened phase formed in situ during high-temperature sintering. Point 2 in Fig. 5(c) is a typical layered structure, and its molar ratio of Ti:Al is close to a typical layered TiAl intermetallic compound. Combined with the XRD results, these results indicated a mixed phase of TiAl and Ti_3Al. The molar ratio of Ti:Al at Point 3 in Fig. 5(c) was approximately 1:1, corresponding to the TiAl matrix phase of the material. According to the point scanning analysis results and Figs. 5(d–f), the Ti_2AlN-reinforced phase was distributed uniformly in the composite as a continuous network, indicating the successful preparation of a Ti_2AlN/TiAl composite with a new network structure by gas nitriding and SPS of the TiAl pre-alloyed powder.

Statistical analysis of the reinforced phase content of the three composites (Figs. 6(a−c)) showed that with the increase in nitriding time, the structure of the reinforced phase structure changed from discontinuous to continuous, and the thickness increased; the highest content (volume fraction) of

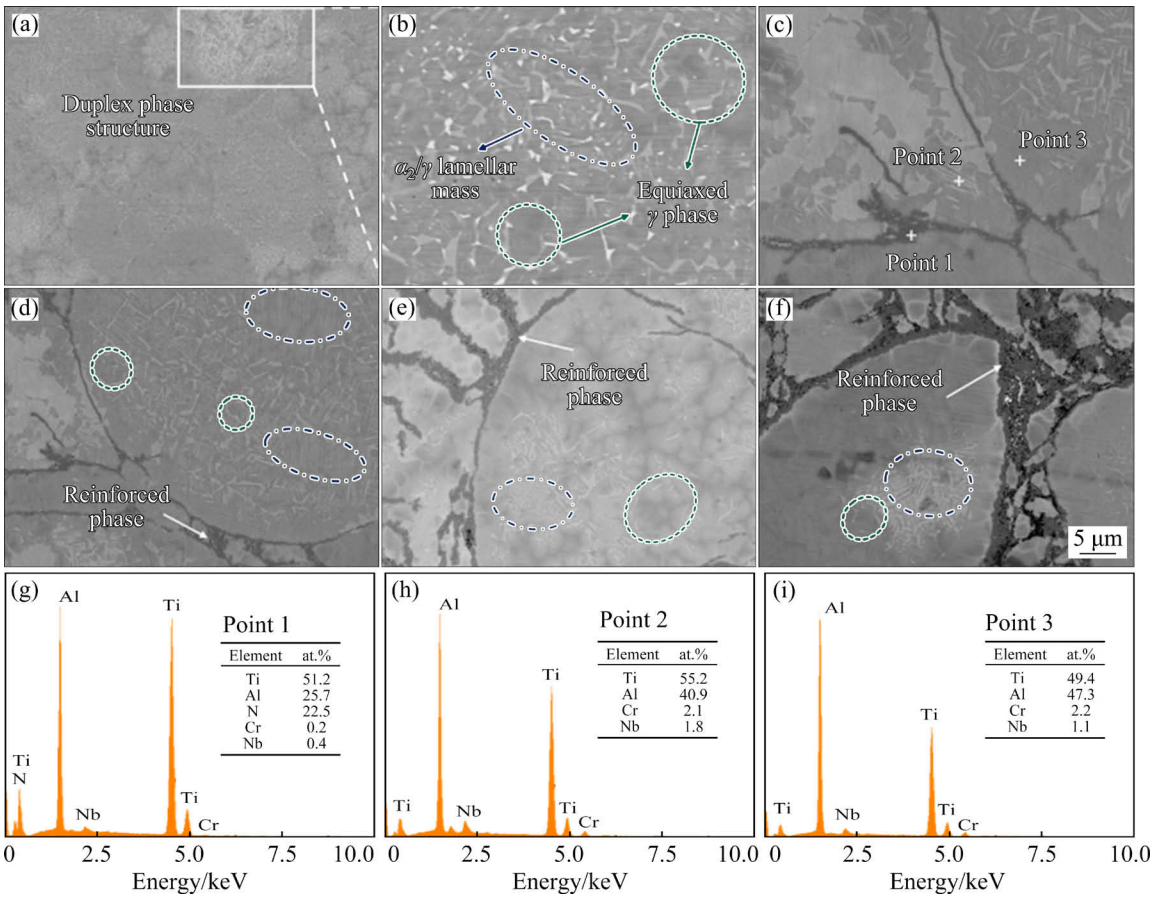

Fig. 5 Microstructures of TiAl alloy and sintered composites: (a, b) TAN-0 h; (c, d) TAN-2 h; (e) TAN-4 h; (f) TAN-8 h; (g−i) EDS patterns of Points 1, 2 and 3 in (c)

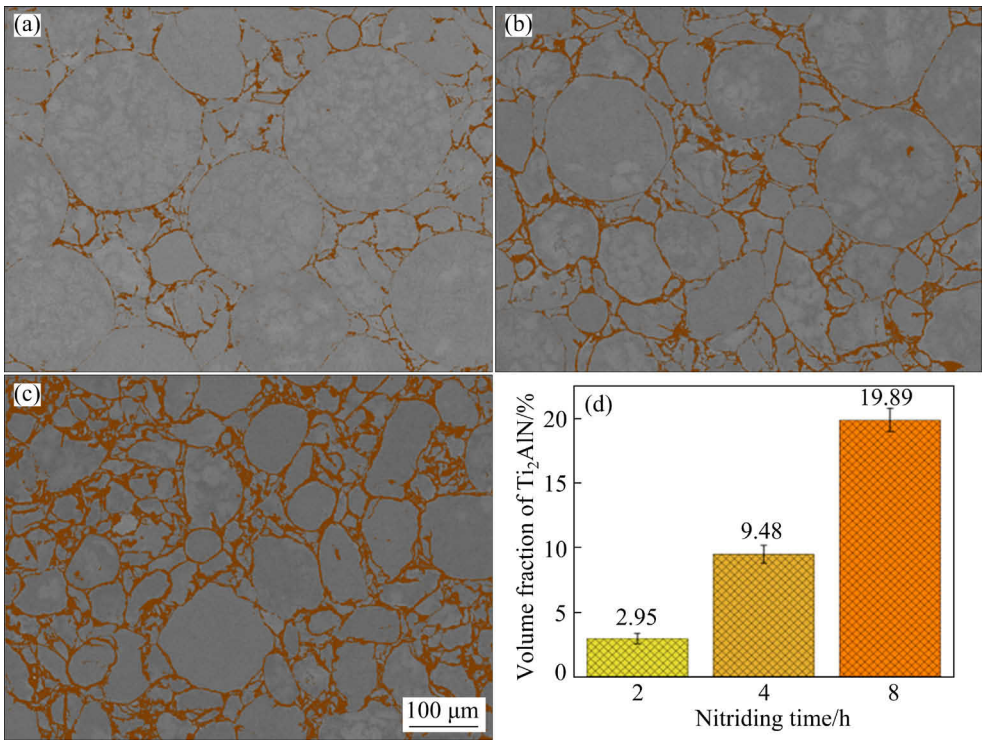

Fig. 6 Statistical analysis results of Ti_2AlN-reinforced phase distribution and phase content in composites: (a) TAN-2 h; (b) TAN-4 h; (c) TAN-8 h; (d) Volume fraction of reinforced phase

the reinforced phase was 19.89% and the lowest was 2.95%. Additionally, as shown in Fig. 6, the reinforced phase was present in two distribution states: TiAl matrix surrounded by the Ti_2AlN reinforced phase with a continuous network structure and a small part of the reinforced phase pinned in the TiAl matrix in granular form. In order to further quantitatively characterize the nitrogen content in nitrided powder corresponding to different nitriding time, oxygen−nitrogen−hydrogen analyzer (ONH836) was used for quantitative test. The mass fraction of nitrogen in powder after nitriding for 2, 4 and 8 h was 0.32%, 0.96% and 2.1%, respectively.

As shown in Fig. 7, EDS analysis was used for TAN-2 h to analyze its composition. Figure 7(a) shows the results of the line scan composition analysis, where the line scanning area passes through the matrix and network structure. The results show that when passing through the network structure, the intensities of Ti and N increase, while the intensity of Al decreases, and the decrease for Al is greater than the increase for Ti and N, corresponding to the element change from the TiAl phase to the Ti_2AlN phase. Figure 7(b) shows the results of the surface scanning composition analysis, where N is mainly enriched in the network structure at the boundary of the TiAl matrix phase, where Al is deficient and the content of Ti slightly increases. In the area outside the network structure, the contents of Al and Ti are significantly higher. Different elements have different light and dark distributions in the TiAl matrix phase, indicating that the composition of each element fluctuates alternately in the equiaxed γ grain and γ/α_2 lamellar clusters in the matrix structure.

The TAN-8 h composite was studied using TEM to further understand the distribution and growth morphology of the reinforced phase and matrix structure; the results are shown in Fig. 8. Figures 8(a−c) show bright-field TEM images, and Figs. 8(d, e) correspond to the SAED of Points 1 and 2 in Figs. 8(a, b), respectively. EDS component analysis was also carried out for Points 1 and 2. According to the EDS and SAED results, the reinforced phase was Ti_2AlN and the matrix phase was TiAl. Figures 8(a−c) show that the reinforced phase has two distribution forms: the Ti_2AlN phase surrounding the TiAl matrix in a continuous network structure (Fig. 8(a)) and the Ti_2AlN phase pinned in the TiAl matrix in granular form (Fig. 8(c)). The layered structure in the TiAl matrix can also be observed in Fig. 8(b), which is consistent with the SEM results (microstructure and morphology) of the composites in the previous section. In addition, there are three forms of the growth of the granular Ti_2AlN-reinforced phase: equiaxed, rod, and hexagonal [15,29,38]. Figure 8(f) shows a high-resolution image of the Ti_2AlN-strengthened phase with the atoms presenting an obvious layered arrangement, consistent with the characteristics of Ti_2AlN ternary layered compounds. The measurements showed that the lattice spacing of the Ti_2AlN phase was 0.844 nm.

3.2 Room temperature and high-temperature hardness of sintered composites

The Vickers hardness of the composites at different temperatures is shown in Fig. 9, which shows the relationship between the hardness of the composites, nitriding time, and test temperature. As shown in Fig. 9, with an increase in nitriding time

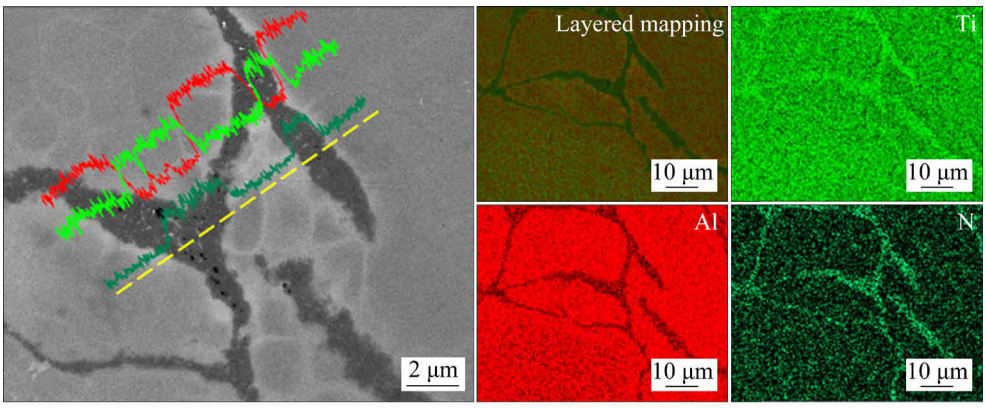

(a) (b)

Fig. 7 SEM−EDS results of TAN-2 h composite: (a) Line scanning; (b) Surface scanning

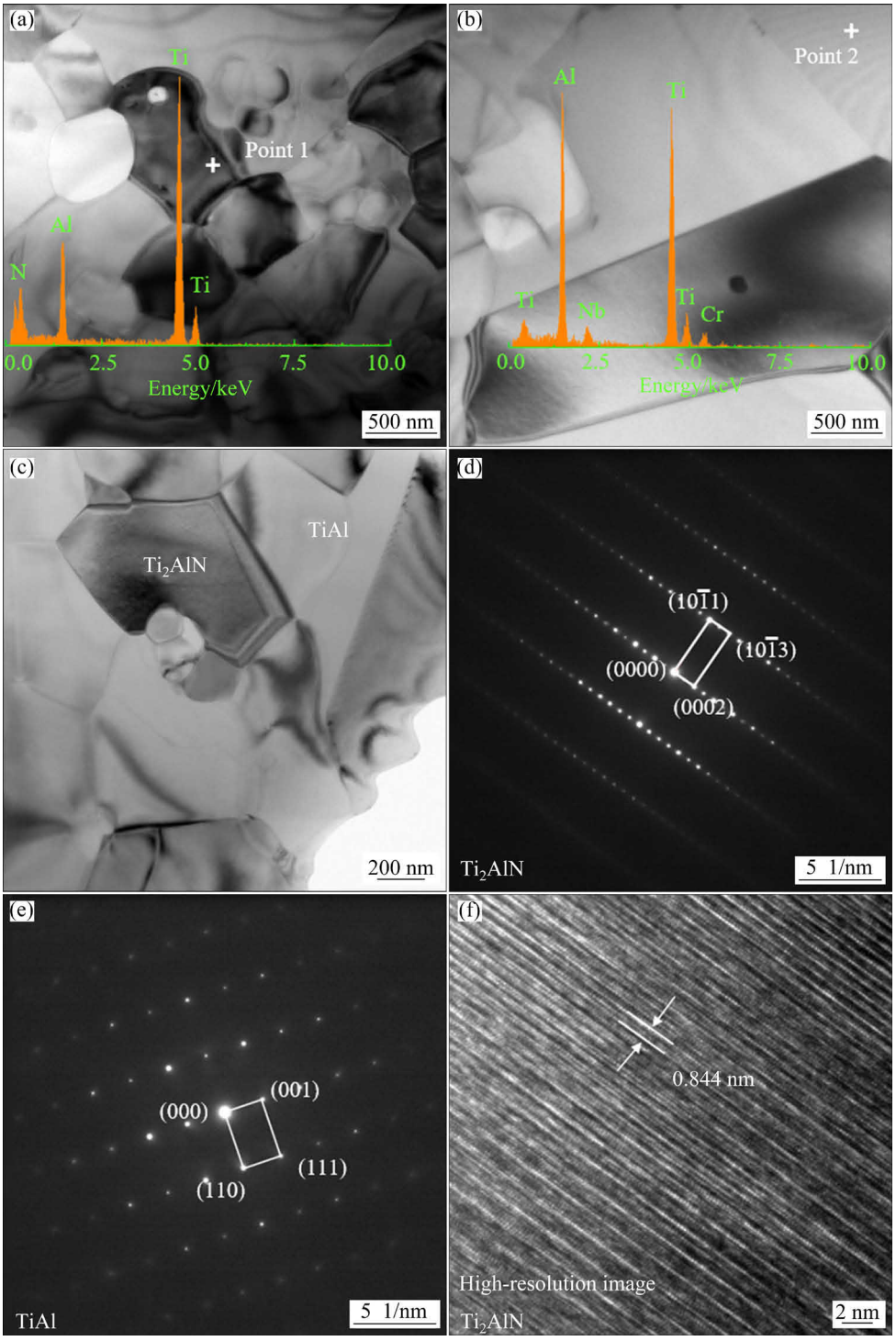

Fig. 8 TEM results of TAN-8 h composite: (a−c) TEM images; (d, e) SAED patterns of matrix phase and reinforced phase, respectively; (f) HRTEM image of reinforced phase

from 0 to 8 h, the hardness of the TAN composites steadily increased; at room temperature, the hardness of the composites increased by 53% (from HV 322 to HV 492). At high temperatures, the hardness of the TAN composites was also greatly improved. The highest improvement was observed in the hardness of TAN-8 h, a 63% increase (from HV 215 to HV 351) at 600 °C. The results show that the new process proposed in this study successfully improved the hardness of the TAN composites at different temperatures. This achievement will potentially promote the application of TiAl in high-temperature structural materials.

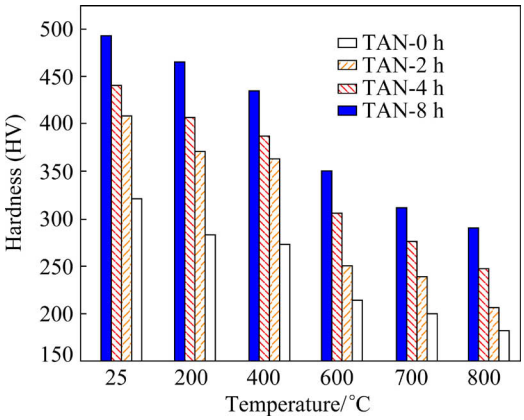

Fig. 9 Room temperature and high-temperature hardness of Ti_2AlN/TiAl composites and TiAl alloys

The strengthening effect of Ti_2AlN/TiAl composites was induced by a series of strengthening mechanisms caused by nitriding and the Ti_2AlN-reinforced phase. The Ti_2AlN phase has a higher elastic modulus and hardness than the TiAl alloy matrix [39]; therefore, Ti_2AlN is the main bearing phase when the external load contacts and destroys the material. Moreover, the reinforced phase can also hinder crack propagation by increasing the crack path or consuming crack propagation energy through tearing [40], explained by the shear lag model adopted by FANG et al [35]. Further, according to the dislocation density formula (Eq. (1)), the difference in the thermal expansion coefficient is directly proportional to the dislocation density, while the thermal expansion coefficients of the TiAl matrix material and Ti_2AlN-reinforced phase are different [41]. Therefore, introducing the Ti_2AlN reinforced phase increases the dislocation density and further affects the hardness of the material [42]. The TEM image of TAN-8 h shows that the yellow mark in Fig. 10(a) is the clean bonding interface of the TiAl matrix without the Ti_2AlN-reinforceed phase, with no dislocations and stacking faults. However, from the white marks in Figs. 10(a, b), it can be observed that there are large numbers of stacking faults, dislocations, and dislocation pinning at the bonding interface between the Ti_2AlN-reinforced phase and TiAl matrix phase. This phenomenon further proves that introducing the Ti_2AlN-reinforced phase leads to an increase in dislocation density, thus improving the hardness of the material.

$$\rho = \frac{12\Delta\alpha\Delta T\upsilon_p}{bd_p(1-\upsilon_p)} \quad (1)$$

where ρ is the dislocation density, d_p is the particle size of the reinforcement, $\Delta\alpha$ is the difference in the thermal expansion coefficient between TiAl and the reinforced phase, ΔT is the difference between the processing and room temperatures, b is the amplitude of Burgers vector, and υ_p is the Poisson ratio of precipitate.

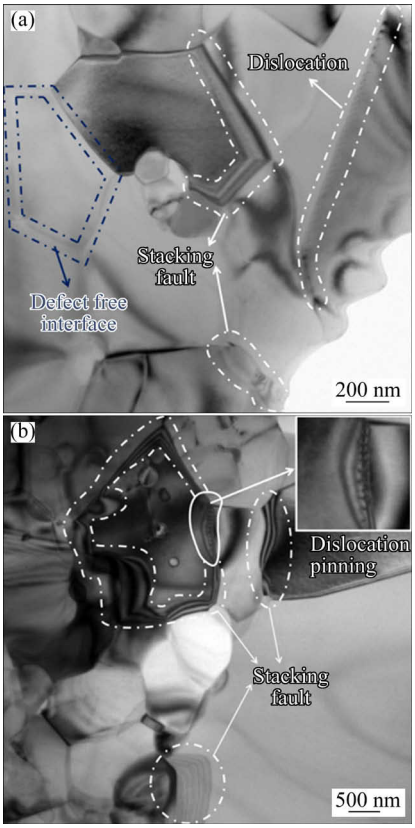

Fig. 10 TEM images of TAN-8 h composite: (a) Excellent binding interface and defective interface between matrix phase and reinforced phase; (b) Dislocation pinning and stacking faults between interfaces of matrix phase and reinforced phase

Further, the XRD analysis of the nitriding process of the TiAl pre-alloyed powder in Fig. 3(b) shows that the main characteristic diffraction peak of the TiAl alloy powder shifts after nitriding, and the degree of shift increases with increasing nitriding time. This is because, during nitriding, in addition to the formation of nitrides on the powder surface, some of the N atoms dissolved in the lattice of the alloy cause lattice distortion, resulting in the shift of the characteristic diffraction peak of the material [41]. Moreover, the solid solution phenomenon further enhances solid solution strengthening and improves the hardness of the TAN composite.

Figure 9 shows that although the nitriding time increases exponentially, at room temperature, only the hardness of TAN-2 h increases significantly, while the hardness increment of TAN-4 h and TAN-8 h slows down. Based on the above analysis of the strengthening mechanism, the reason for this phenomenon may be that with the increase in nitriding time, the solid solution strengthening and the increased dislocation density reach saturation, after which the increase in hardness is mainly caused by the bearing effect of a higher volume fraction of the reinforced phase; thus, the overall growth has little difference.

In addition to the effect of nitriding time on hardness, temperature also significantly affects the hardness of the composites. As shown in Fig. 9, with an increase in temperature, the hardness of the composites decreased continuously, explained by Eqs. (2) and (3) proposed by HISOKIN, and SHERBY and ARMSTRONG, respectively. Both the above expressions prove that the hardness of the material is an exponentially decreasing function of temperature [43,44]; therefore, the hardness of TAN composites continues to decrease with an increase in temperature. Simultaneously, the hardness of the TiAl alloy and its three composites decreases significantly at 600 °C. In addition to the fact that the hardness is inversely proportional to the temperature, it may also be related to the ductile–brittle transition temperature of TiAl alloy. As the ductile–brittle transition temperature of the TiAl alloy is 600−820 °C [45], the material may change from brittleness to toughness at approximately 600 °C, resulting in poor deformation resistance and a decrease in hardness.

$$H=A\exp(-BT) \quad (2)$$

$$H=A\exp(B/T) \quad (3)$$

where H is the hardness, A and B are constants, and T is the temperature.

In general, the hardness of TAN-8 h was higher than that of the TiAl alloy at 600, 700, and 800 °C by 63%, 54%, and 59%, respectively. This result provided the basic data for using these composites for high-temperature parts of aerospace equipment. In this study, a new process of nitriding and sintering TiAl pre-alloyed powder, potentially expanding the structural design of TiAl composites, was proposed. Therefore, in the next section, the room-temperature compression properties of TAN composites were tested. The compression and fracture properties of the TAN composites were further analyzed through the compression fracture morphology.

3.3 Compression and fracture properties of sintered composites

Figure 11(a) shows the compressive stress–strain curves of the TAN composite, which are divided into three parts. In the early stage of deformation, the flow stress increases and shows strain hardening; then, the stress gradually increases, and finally, fracture occurs. With the increase in nitriding time, the compressive strain of the material gradually decreases. Based on the results in the previous section, the reason may be that the increase in the hardness of TAN composite leads to a decrease in material plasticity to a certain extent. As shown in Fig. 11(b), with the increase in nitriding time, the compressive strength of the TAN composite also decreases, especially for TAN-4 h, possibly because a large number of the reinforced

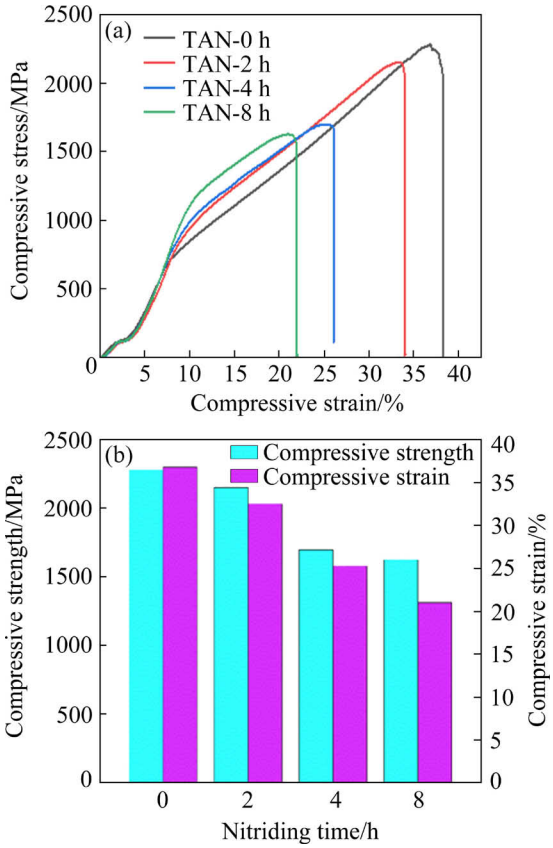

Fig. 11 Compressive properties of Ti_2AlN/TiAl composites and TiAl alloys: (a) Compressive stress–strain curves; (b) Ultimate compressive strength and compressive strain

phases were formed in the composites, leading to an increase in the material brittleness, which are consistent with the conclusions of LIU et al [33].

The compressive strengths of TAN-4 h and TAN-8 h exhibited little difference. Combined with the microstructure of the composites, this finding shows that the composites, after nitriding for 4 h, formed a continuous network of the reinforced phase, improving the hardness of the materials and reducing their plasticity; compared with nitriding for 4 h, nitriding for 8 h only thickened the network structure of the reinforced phase. Therefore, there was little difference in the overall compressive strength between the TAN-4 h and TAN-8 h phases. Importantly, although the compressive strength and compressive strain of the TAN composites were lower than those of the original TiAl pre-alloyed powder sintered using the same process (shown in Fig. 11(b)), their maximum compressive strength reached 2279 MPa, and the maximum compressive strain was as high as 36.78%.

Figure 12 shows the compressive fracture morphologies of TAN-0 h, TAN-2 h, and TAN-8 h at room temperature. In the compressive fracture shown in Fig. 12(a), crack propagation can be clearly observed in TAN-0 h; moreover, intergranular propagation, transgranular propagation, and microcracks were observed in the main crack propagation process, indicating that the matrix structure of the TiAl alloy cannot stop crack propagation. Figures 12(b, c) show the high-magnification images of the fracture features. There is a large area of characteristic morphology similar to intergranular fracture and cleavage surface formed by partial dissociation fracture on the fracture surface; in addition, river-like characteristic patterns can be observed on some cleavage surfaces. There are also through-layer fractures in the matrix layered structure and some layered distortion morphology caused by an external force. The above characteristics show that the fracture mode of TAN-0 h is mainly brittle fracture, with small amount of plastic deformation in some parts.

Figures 12(d−f) show the fracture morphologies of TAN-2 h. The honeycomb structure in Fig. 12(d) was analyzed by EDS to determine the

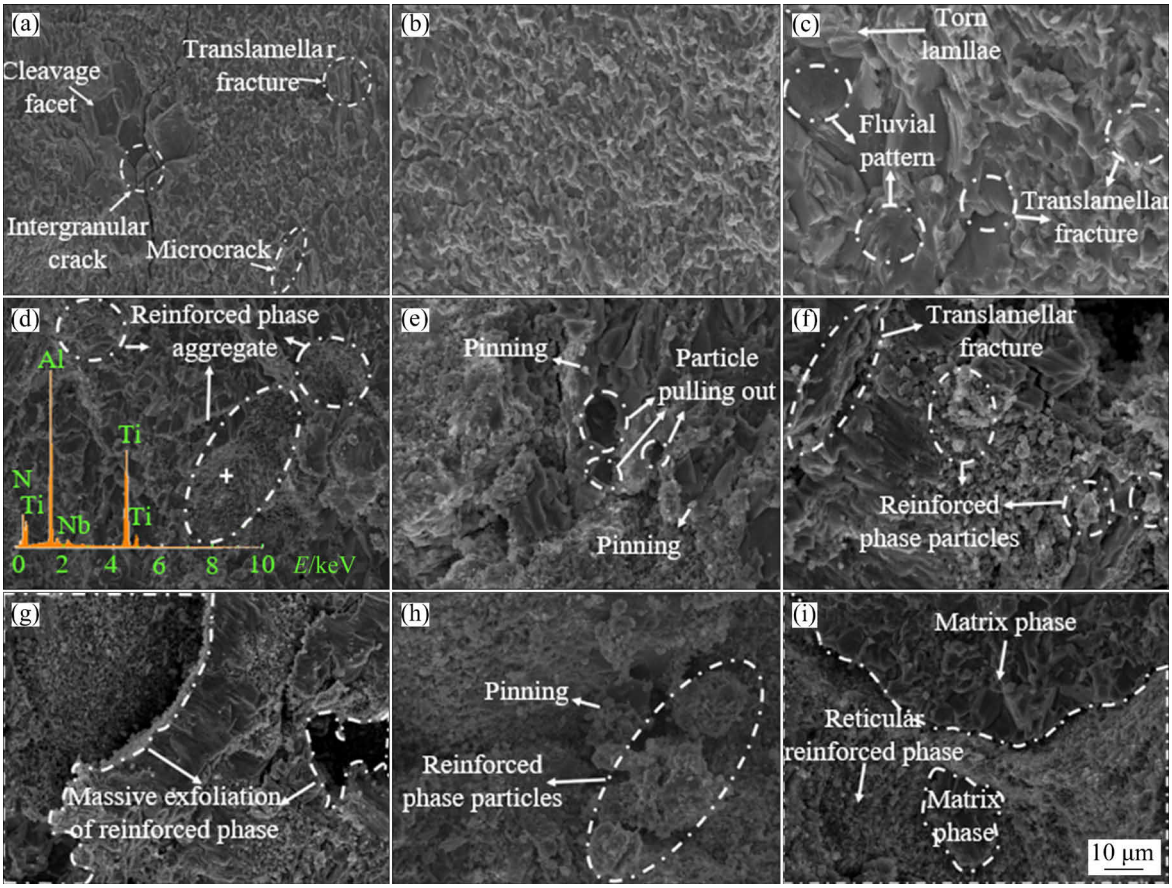

Fig. 12 Compressioven fracture morphologies of Ti_2AlN/TiAl composites and TiAl alloys: (a−c) TAN-0 h; (d−f) TAN-2 h; (g−i) TAN-8 h

phase composition of different fracture morphologies. The results show that the honeycomb structure is a Ti_2AlN-reinforced phase, the remaining cleavage structure is the TiAl matrix phase, and the reinforced phase structure of TAN-2 h is discontinuous. The pinning and pulling out of the reinforced phase particles can be seen in the high-magnification images in Figs. 12(e, f). Moreover, there are characteristic morphologies of intergranular fracture and through-layer fracture, and some broken reinforced phase particles can be seen at the crack propagation. Figures 12(g–i) show the fracture morphology of TAN-8 h. Figure 12(g) shows that there are large pieces of the reinforced phases that fall off; too many reinforced phases are not conducive to improving the comprehensive mechanical properties of the Ti_2AlN/TiAl composites [31,46]. Figures 12(h, i) show two forms of TAN-8 h after compression fracture, i.e., the continuous mesh-reinforced phase and dispersed particles after crushing of the mesh-reinforced phase.

Figures 13(a−c) show the fracture morphology of the compressed sample surface after corrosion. Figure 13(d) shows bright-field TEM image. Figures 13(e, f) show HRTEM images of the phase boundary between the reinforced phase and the matrix phase. Given that the compressive strength decreases with an increase in the hardness of composites, this study analyzed this phenomenon in combination with SEM images, TEM images, and literature research. The main reasons for this may be as follows.

Firstly, because of the inherent brittleness of the reinforced phase [47,48], the analysis of hardness and compressive strength in the previous section showed that the hardness of the composite in this study increased simultaneously with brittleness to a certain extent.

Secondly, ZHANG et al [46] found that the formation of a large-area network of the reinforced phase often leads to the emergence of pores. Figure 13 shows that the cracks in the composite materials often start at the holes where the reinforced phase is not closely combined with the matrix. The main cracks commonly expand along the interface between the Ti_2AlN particles and matrix structure, resulting in poor bonding. Although the reinforced phase deflected cracks, stopped cracks, and tore the reinforced phase to prevent crack propagation, the overall compressive strength of the material still decreased.

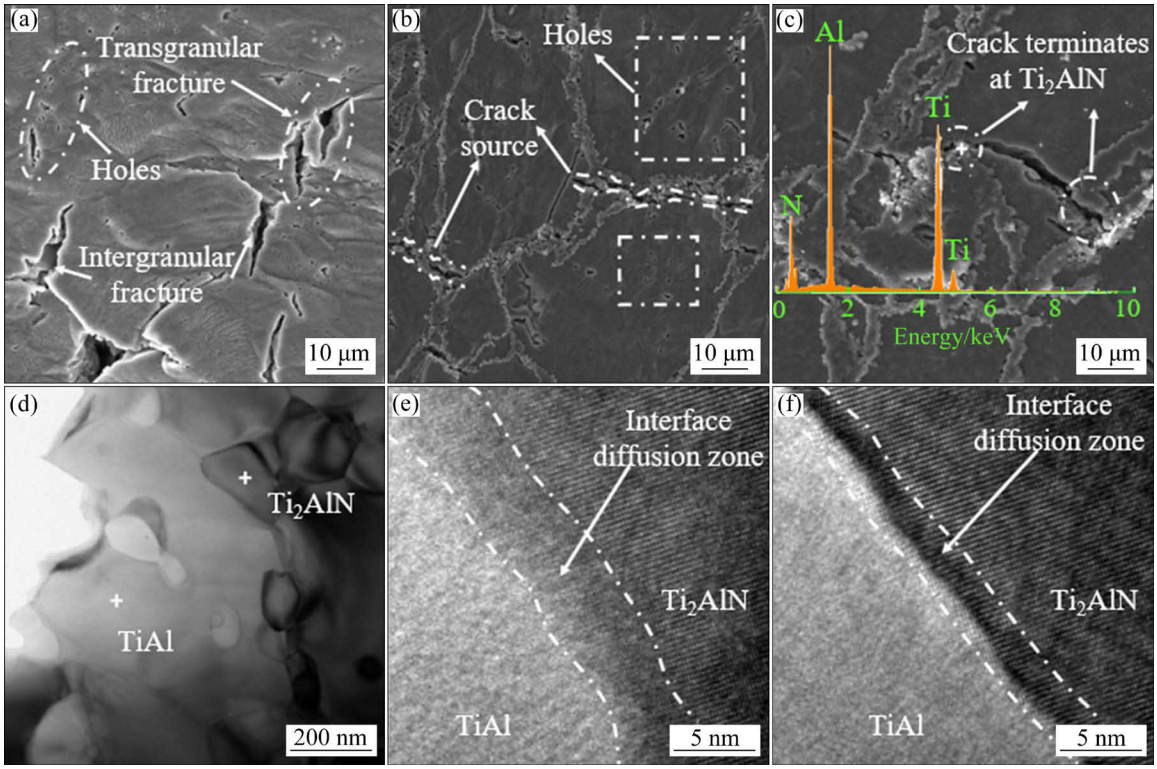

Fig. 13 Fracture morphologies of TAN-0 h (a), TAN-2 h (b) and TAN-8 h (c) composites after corrosion, TEM image of TAN-8 h composite (d) and HRTEM image of composite TAN-8 h (e, f)

Thirdly, CUI et al [49] found that the mismatch of the thermal expansion coefficient and weak self-adhesive strength between the two phases leads to an increase in residual stress and deterioration of interphase bonding. As seen in Figs. 13(e, f), there are two interface bonding states between the reinforced phase and the matrix structure, in which the bonding interface in Fig. 13(e) has an interface diffusion bonding area; thus, the interface is smooth and clean, and the bonding strength is excellent [41]. However, the bonding interface in Fig. 13(f) is poor, thus unfavorable to strong bonding between the two phases. The former is the Ti_2AlN-reinforced phase formed in situ from the TiN phase produced after the nitriding of the powder during sintering, and the latter is a small part of the Ti_2AlN particles directly formed during the nitriding of the powder. In conclusion, the latter leads to a decrease in the compressive properties of the composites. Therefore, in future research, more appropriate preparation process parameters need to be further explored to obtain excellent comprehensive properties.

4 Conclusions

(1) Nitrogen was introduced into TiAl pre-alloyed powder using high-temperature gas nitriding, and Ti_2AlN/TiAl composites with a continuous network structure of the reinforced phase were prepared via SPS.

(2) The continuous network Ti_2AlN phase in Ti_2AlN/TiAl composites is composed of Ti_2AlN phase produced in situ during the SPS sintering process and Ti_2AlN particles produced during the high temperature gas nitriding process. The former was conducive to sintering bonding and densification of the composites, whereas the latter was not.

(3) The hardness of the Ti_2AlN/TiAl composites after nitriding for 8 h was the highest irrespective of the temperature. The most significant increase in hardness was observed at 600 °C, i.e., hardness of HV 351, 63% higher than that of the TiAl alloy.

(4) The bearing effect of the continuous network of the Ti_2AlN phase with high hardness and elastic modulus, the dislocation density increased by the differences in the coefficients of thermal expansion, and the mechanism of solid solution strengthening caused by the nitriding of the powder were the main reasons for the significant improvement in the hardness of the composites.

(5) The compressive strength of the Ti_2AlN/TiAl composites was lower than that of the TiAl alloy prepared using the same parameters, preliminarily attributed to the weak bonds between the matrix phase and a part of Ti_2AlN particles directly formed after nitriding, the inherent brittleness of the part of Ti_2AlN particles, and the pore defects caused by a part of Ti_2AlN particles.

Acknowledgments

The authors are grateful for the financial supports from the Cultivation Project for Original Scientific Research Instruments and Equipments of Southwest Jiaotong University, China (No. XJ2021KJZK041), the Key Laboratory of Infrared Imaging Materials and Detectors, Shanghai Institute of Technical Physics, Chinese Academy of Sciences (No. IIMDKFJJ-19-08), and the China Postdoctoral Science Foundation (No. 2018T110993)

References

[1] KUMARAN S, CHANTAIAH B, RAO T S. Effect of niobium and aluminium additions in TiAl prealloyed powders during high-energy ball milling [J]. Materials Chemistry and Physics, 2008, 108: 97−101.

[2] CHU Yu-dong, LI Jin-shan, ZHAO Feng-tong, TANG Bin, KOU Hong-chao. Characterization of the elevated temperature compressive deformation behavior of high Nb containing TiAl alloys with two microstructures [J]. Materials Science and Engineering A, 2018, 725: 466−478.

[3] KOTHARI K, RADHAKRISHNAN R, WERELEY N M. Advances in gamma titanium aluminides and their manufacturing techniques [J]. Progress in Aerospace Sciences, 2012, 55: 1−16.

[4] LIU Zhan-qi, MA Rui-xin, XU Guo-jian, WANG Wen-bo, SU Yun-hai. Effects of annealing on microstructure and mechanical properties of γ-TiAl alloy fabricated via laser melting deposition [J]. Transactions of Nonferrous Metals Society of China, 2020, 30: 917−927.

[5] YANG Yong, FENG He-ping, WANG Qi, CHEN Rui-run, GUO Jing-jie, DING Hong-sheng, SU Yan-qing. Improvement of microstructure and mechanical properties of TiAl−Nb alloy by adding Fe element [J]. Transactions of Nonferrous Metals Society of China, 2020, 30: 1315−1324.

[6] CHENG Jun, LI Fei, FU Li-cai, QIAO Zhu-hui, YANG Jun, LIU Wei-min. Dry-sliding tribological properties of TiAl/Ti_2AlC composites [J]. Tribology Letters, 2014, 53: 457−467.

[7] FOROUZANMEHR N, KARIMZADEH F, ENAYATI M H.

Study on solid-state reactions of nanocrystalline TiAl synthesized by mechanical alloying [J]. Journal of Alloys and Compounds, 2009, 471: 93−97.

[8] NIU H Z, GAO T X, SUN Q Q, ZHANG H R, ZHANG D L, LIU G L. Prior particle boundaries and microstructural homogenization of a β-solidifying γ-TiAl alloy fabricated from prealloyed powder [J]. Materials Science and Engineering A, 2018, 737: 151−157.

[9] YANG Yu-ling, ZHANG Duo, YAN Wei, ZHENG Yi-ran. Microstructure and wear properties of TiCN/Ti coatings on titanium alloy by laser cladding [J]. Optics and Lasers in Engineering, 2010, 48: 119−124.

[10] TAN Ying-mei, CHEN Rui-run, LIU Yang-li, DING Hong-sheng, SU Yan-qing, GUO Jing-jie, FU Heng-zhi. Formation of Ti_2AlN and TiB and its effect on mechanical properties of $Ti_{46}Al_4Nb_1Mo$ alloy by adding BN particles [J]. Materials Science and Engineering A, 2019, 756: 161−171.

[11] LIU Yi, LI Ying-xin, LI Fan, CUI Han, ZHANG Li-feng, GUO Shou-wu. Synthesis and microstructure of Ti_2AlN ceramic by thermal explosion [J]. Ceramics International, 2017, 43: 13618−13621.

[12] SUN Z M. Progress in research and development on MAX phases: A family of layered ternary compounds [J]. International Materials Reviews, 2011, 56: 143−166.

[13] CHING W Y, MO Y X, ARYAL S, RULIS P. Intrinsic mechanical properties of 20 MAX-phase compounds [J]. Journal of the American Ceramic Society, 2013, 96: 2292−2297.

[14] DUONG T, GIBBONS S, KINRA R, ARROYAVE R. Ab-initio aprroach to the electronic, structural, elastic, and finite-temperature thermodynamic properties of Ti_2AX (A= Al or Ga and X=C or N) [J]. Journal of Applied Physics, 2011, 110: 093504.

[15] ZHOU Yi, SUN Dong-Li, WANG Qing, HAN Xiu-Li. Effect of fabrication parameters on the microstructure and mechanical properties of unidirectional Mo-fiber reinforced TiAl matrix composites [J]. Materials Science and Engineering A, 2013, 575: 21−29.

[16] HUANG L J, GENG L, PENG H X, ZHANG J. Room temperature tensile fracture characteristics of in situ TiB_w/Ti_6Al_4V composites with a quasi-continuous network architecture [J]. Scripta Materialia, 2011, 64: 844−847.

[17] FRATZL P, GUPTA H S, PASCHALIS E P, ROSCHGER P. Structure and mechanical quality of collagen−mineral nano-composite in bone [J]. Journal of Materials Chemistry, 2004, 14: 2115−2123.

[18] HUANG L J, GENG L, FU Y, KAVEENDRAN B, PENG H X. Oxidation behavior of in situ TiC_p/Ti_6Al_4V composite with self-assembled network microstructure fabricated by reaction hot pressing [J]. Corrosion Science, 2013, 69: 175−180.

[19] JIAO Y, HUANG L J, WANG S, LI X T, AN Q, CUI X P, GENG L. Effects of first-scale TiB_w on secondary-scale Ti_5Si_3 characteristics and mechanical properties of in-situ $(Ti_5Si_3+TiB_w)/Ti_6Al_4V$ composites [J]. Journal of Alloys and Compounds, 2017, 704: 269−281.

[20] TRZASKA Z, BONNEFONT G, FANTOZZI G, MONCHOUX J P. Comparison of densification kinetics of a TiAl powder by spark plasma sintering and hot pressing [J]. Acta Materialia, 2017, 135: 1−13.

[21] VOISIN T, MONCHOUX J P, DURANT L, KARNATAK N, THOMAS M, COURET A. An innovative way to produce γ-TiAl blades: Spark plasma sintering [J]. Advanced Engineering Materials, 2015, 17: 1408−1413.

[22] BHATTACHARYA P, BELLON P, AVERBACK R S, HALES S J. Nanocrystalline TiAl powders synthesized by high- energy ball milling: Effects of milling parameters on yield and contamination [J]. Journal of Alloys and Compounds, 2004, 368: 187−196.

[23] GUYON J, HAZOTTE A, MONCHOUX J P, BOUZY E. Effect of powder state on spark plasma sintering of TiAl alloys [J]. Intermetallics, 2013, 34: 94−100.

[24] BOES J, RÖTTGER A, BECKER L, THEISEN W. Processing of gas-nitrided AISI 316L steel powder by laser powder bed fusion — Microstructure and properties [J]. Additive Manufacturing, 2019, 30: 100836.

[25] SHA W, DON M, MOHAMED A, WU X, SILIANG B, ZHECHEVA A. X-ray diffraction, optical microscopy, and microhardness studies of gas nitrided titanium alloys and titanium aluminide [J]. Materials Characterization, 2008, 59: 229−240.

[26] VAJPAI S K, AMEYAMA K. A novel powder metallurgy processing approach to prepare fine-grained Ti-rich TiAl-based alloys from pre-alloyed powders [J]. Intermetallics, 2013, 42: 146−155.

[27] BOUOUDINA M, LUKLINSKA Z, GUO Z X. Effect of milling conditions on structural evolution and phase stability of $[Ti(H_2)+Al+Nb]$ powder mixtures [J]. Materials Science and Engineering A, 2008, 474: 173−180.

[28] WANG Y X, ZHANG K F, LI B Y. Microstructure and high temperature tensile properties of $Ti_{22}Al_{25}Nb$ alloy prepared by reactive sintering with element powders [J]. Materials Science and Engineering A, 2014, 608: 229−233.

[29] SUN D L, SUN T, WANG Q, HAN X L, GUO Q, WU G H. Fabrication of in situ Ti_2AlN/TiAl composites by reaction hot pressing and their properties [J]. Journal of Wuhan University of Technology: Materials Science Edition, 2014, 29: 126−130.

[30] BARS J P, DAVID D, ETCHESSAHAR E, DEBUIGNE J. Titanium α-nitrogen solid solution formed by high temperature nitriding: diffusion of nitrogen, hardness, and crystallographic parameters [J]. Metallurgical & Materials Transactions A, 1983, 14: 1537−1543.

[31] WANG D Q, SUN D L, HAN X L, WANG Q. In situ Ti_2AlN reinforced TiAl-based composite with a novel network structure: Microstructure and flexural property at elevated temperatures [J]. Materials Science and Engineering A, 2019, 742: 231−240.

[32] ROY A, KUMAR K S, RAGHUNATH A, SHARMA R C, SHEKHAR R. Feasibility and kinetics of nitriding of pure titanium and Ti−6Al−4V in molten salt bath of potassium nitrate [J]. Surface Engineering, 2012, 28: 458−463.

[33] LIU Y, HU R, ZHANG T, KOU C H, LI J. Microstructure characterization and mechanical properties of in situ synthesized $Ti_2AlN/Ti_{48}Al_2Cr_2Nb$ composites [J]. Advanced Engineering Materials, 2014, 16: 507−510.

[34] MCCULLOUGH C, VALENCIA J J, LEVI C G, MEHRABIAN R. Phase equilibria and solidification in

Ti−Al alloys [J]. Acta Metallurgica, 1989, 37: 1321−1336.
[35] FANG H Z, CHENR R, YANG Y, SU Y Q, DING H S, GUO J J, FU H Z. Role of graphite on microstructural evolution and mechanical properties of ternary TiAl alloy prepared by arc melting method [J]. Materials & Design, 2018, 156: 300−310.
[36] CHEN Y L, YAN M, SUN Y M, MEI B C, ZHU J Q. The phase transformation and microstructure of TiAl/Ti_2AlC composites caused by hot pressing [J]. Ceramics International, 2009, 35: 1807−1812.
[37] VISWANATHAN G B, VASUDEVAN V K. Processing, microstructure and tensile properties of a Ti−48at.%Al alloy [J]. Scripta Metallurgica et Materialia, 1995, 32: 1705−1711.
[38] WANG D Q, SUN D L, HAN X L, WANG Q, ZHANG N B, XU F B. Fabrication and mechanical properties of in situ synthesized Ti_2AlN/TiAl composite [J]. Journal of Materials Engineering and Performance, 2018, 27: 4336−4344.
[39] ZHANG J Y, KE W X, WEI J, ZHANG F, WANG W M, FU Z Y. Microstructure and properties of in situ titanium boride (TiB)/titanium (Ti) composites [J]. Materials Science and Engineering A, 2015, 648: 158−163.
[40] LIU Y W, HU R, YANG J R, LI J. Tensile properties and fracture behavior of in-situ synthesized Ti_2AlN/$Ti_{48}Al_2Cr_2Nb$ composites at room and elevated temperatures, [J]. Materials Science and Engineering A, 2017, 679: 7−13.
[41] ZHU J F, YANG W W, YANG H H, WANG F. Effect of Nb_2O_5 on the microstructure and mechanical properties of TiAl based composites produced by hot pressing [J]. Materials Science and Engineering A, 2011, 528: 6642−6646.
[42] DING R F, WANG H, JIANG Y, LIU R, LIU C. Effects of ZrC addition on the microstructure and mechanical properties of Fe−Cr−Al alloys fabricated by spark plasma sintering [J]. Journal of Alloys and Compounds, 2019, 805: 1025−1033.
[43] KEYVANI M, MAHMUDI R, NAYYERI G. Effect of Bi, Sb, and Ca additions on the hot hardness and microstructure of cast Mg−5Sn alloy [J]. Materials Science and Engineering A, 2010, 527: 7714−7718.
[44] RAJAN K, SARMA V S, KUTTY T R G, MURTY B S. Hot hardness behaviour of ultrafine grained ferritic oxide dispersion strengthened alloys prepared by mechanical alloying and spark plasma sintering [J]. Materials Science and Engineering A, 2012, 558: 492−496.
[45] WANG Y, LIN D L. Brittle-to-ductile transition temperature and its strain rate sensitivity in a two-phase titanium aluminide with near lamellar microstructure [J]. Journal of Materials Science, 1999, 34: 3155−3159.
[46] ZHANG L G, LUO X, LIU J L, LRNG Y X, AN L N. Dry sliding wear behavior of Mg−SiC nanocomposites with high volume fractions of reinforcement [J]. Materials Letters, 2018, 228: 112−115.
[47] DU Y L, SUN Z M, HASHIMOTO H, BARSOUM M W. Theoretical investigations on the elastic and thermodynamic properties of $Ti_2AlC_{0.5}N_{0.5}$ solid solution [J]. Physics Letters A, 2009, 374: 78−82.
[48] CUI X P, FAN G H, GENG L, WANG Y, ZHANG H W, PENG H X. Fabrication of fully dense TiAl-based composite sheets with a novel microlaminated microstructure [J]. Scripta Materialia, 2011, 66: 276−279.
[49] CUI B, SA R, JAYASEELAN D D, INAM F, LEE W E. Microstructural evolution during high-temperature oxidation of spark plasma sintered Ti_2AlN ceramics [J]. Acta Materialia, 2012, 60: 1079−1092.

连续网状结构 Ti_2AlN/TiAl 复合材料的制备及力学性能

蒋闽晋[1,2]，孙红亮[1,2]，刘 瑞[1,2]，蒋小松[1,2]，张亚丽[3]，孙大明[4]

1. 材料先进技术教育部重点实验室，成都 610031；
2. 西南交通大学 材料科学与工程学院，成都 610031;
3. School of Mechanical Engineering, Sungkyunkwan University,
2066 Seobu-ro, Jangan-gu, Suwon-si, Gyeonggi-do, 16419, Korea;
4. Department of Chemistry and Bioscience, Aalborg University, Aalborg, 9220, Denmark

摘 要：采用高温气体渗氮法将氮引入 TiAl 预合金粉末中，然后采用放电等离子烧结法制备具有连续网络增强相结构的 Ti_2AlN/TiAl 复合材料。结果表明，复合材料的硬度明显高于 TiAl 合金的硬度，并随着氮化时间的增加而增加。该强化效果是粉末渗氮引起的固溶体强化、具有高硬度和弹性模量的连续网状 Ti_2AlN 相以及位错密度增加协同作用的结果。同时，与 TiAl 合金相比，Ti_2AlN/TiAl 复合材料的抗压强度降低，这与氮化后直接形成的一部分 Ti_2AlN 颗粒和过多的增强相含量有关。

关键词：预合金粉末；渗氮；Ti_2AlN/TiAl 复合材料；连续网状结构；显微组织；力学性能

(Edited by Wei-ping CHEN)